

Microanatomy of the central myelin portion and transitional zone of the oculomotor and abducens nerves

W. Quanchareonsap¹, S. Jariyakosol², S. Apinyawasisuk², A. Roumwong¹, V. Chentanez¹

¹Department of Anatomy, Faculty of Medicine, Chulalongkorn University, Bangkok, Thailand

²Department of Ophthalmology, Faculty of Medicine, Chulalongkorn University, Bangkok, Thailand

[Received: 18 May 2022; Accepted: 2 June 2022; Early publication date: 10 June 2022]

Background: The microanatomy of the central myelin portion and transitional zone of several cranial nerves including trigeminal, facial, vestibulocochlear, glossopharyngeal, and vagus nerves have been clearly demonstrated to provide information for neurovascular compression syndrome such as trigeminal neuralgia and hemifacial spasm. However, the study of oculomotor and abducens nerve is limited.

Materials and methods: Oculomotor and abducens nerves were harvested with a portion of brainstem and embedded in paraffin. Longitudinal and serial sections from ten of each cranial nerve were stained and a photomicrograph was taken to make the following observations and measurements: 1) patterns of central myelin portion, 2) length of central myelin portion, and 3) depth of central myelin-peripheral myelin transitional zone.

Results: For oculomotor nerve, the longest central myelin bundle was always seen on the first nerve bundle and that the length of central myelin decreased gradually. For abducens nerve, morphological patterns were classified into four types based on number of nerve rootlets emerging from the brainstem and number of nerve bundles in each rootlet. Length of central myelin portion was between 0.36–6.10 mm (2.75 ± 0.83 mm) and 0.13–5.01 mm (1.66 ± 1.39 mm) for oculomotor and abducens nerves, respectively. The oculomotor nerve transitional zone depth was 0.07–0.58 mm (0.23 ± 0.07 mm), while for abducens nerve, depth was 0.05–0.40 mm (0.16 ± 0.07 mm). Positive weak correlations between central myelin and depth of TZ were found in oculomotor nerve ($r +0.310$, $p < 0.05$) and abducens nerves ($r +0.413$, $p < 0.05$).

Conclusions: Detailed microanatomy of the central myelin and transitional zone might be beneficial for locating the site of compression in neurovascular conflicts at oculomotor and abducens nerves. (Folia Morphol 2023; 82, 3: 543–550)

Key words: abducens nerve, central myelin, oculomotor nerve, transitional zone, nerve compression syndrome

Address for correspondence: V. Chentanez, MD, PhD, Department of Anatomy, Faculty of Medicine, Chulalongkorn University, 1873 Rama IV Rd, Khwaeng Pathum Wan, Khet Pathum Wan, Bangkok, Thailand 10330, tel: +66860701084, e-mail: fmedvct@gmail.com

This article is available in open access under Creative Common Attribution-Non-Commercial-No Derivatives 4.0 International (CC BY-NC-ND 4.0) license, allowing to download articles and share them with others as long as they credit the authors and the publisher, but without permission to change them in any way or use them commercially.

INTRODUCTION

Neurovascular compression syndrome is described as direct contact with mechanical irritation of cranial nerves by blood vessels [11]. Compression at the oculomotor and abducens nerves have been reported as a cause of ocular neuromyotonia (ONM) [10, 26, 28] and abducens nerve palsy (CN VI palsy) [2, 6, 7, 12, 13, 15, 16, 18, 19, 21, 30]. ONM is characterised by intermittent, tonic spasms of one or more extraocular muscles. Clinical presentations are strabismus and transient diplopia [23]. Its mechanism is unknown but it has been proposed to be related to neurovascular compression [10, 26, 28]. CN VI palsy is the most common ocular motor paralysis and presents with diplopia. It usually results from neoplasm, trauma, and microvascular ischaemia. It is very rare if vascular compression is considered as the cause [4]. Site of compression is reported variously for both diseases. A cranial nerve consists of central nervous system (CNS) and peripheral nervous system (PNS) segment connected by transitional zone (TZ) [24]. Glial cells in the CNS project distally making a well-defined dome-shaped TZ [22]. The PNS segment has been demonstrated to be more resistance to compression than CNS segment. The TZ is vulnerable since this junction contains both myelin sheaths in the central part produced by oligodendrocytes, and myelin sheaths in peripheral part which are produced by Schwann cells [3]. The difference in the origin of central and peripheral myelin explains the difference in molecular components which contributes to structural differences [1, 14]. The length of central glial segments vary between nerves and differs between each rootlet of the same nerve [25]. The microanatomy of the central myelin portion and TZ of several cranial nerves including trigeminal, facial, vestibulocochlear, glossopharyngeal, and vagus nerves have been clearly demonstrated [8, 9, 17, 20, 27]. However, there were only two previous studies reporting the central myelin portion of oculomotor and abducens nerves [22, 25]. Thus, more microanatomical knowledge of oculomotor nerve and abducens nerve is needed. This study aimed to determine the pattern of central myelin portion, length of central myelin, depth of TZ, and correlation between depth of TZ and length of central myelin of each nerve bundle.

MATERIALS AND METHODS

Twenty-nine oculomotor nerves and 53 abducens nerves were removed with a portion of brainstem

attached from 46 embalmed cadaver brains. The specimens were further fixed in 10% neutral buffered formalin for 24 hours and embedded in paraffin. Each tissue block was longitudinally and serially sectioned into 5 μm thick sections. Only 10 specimens of each cranial nerve were included, the rest were excluded due to poor fixation and detachment of the cranial nerve from the brainstem. First section started where the nerve appeared and last section ended where the whole nerve disappeared. Sections with the nerve still connected to the brainstem were chosen under a light microscope for further staining with luxol fast blue for differentiation of central and peripheral myelin portions. Counterstain with haematoxylin and eosin was performed for better demonstration. Three to six sections with maximum extension of the central myelin from each nerve were chosen under a light microscope for measurement. Axiocam 506 colour microscope camera (Carl Zeiss, Jena, Germany) with a 5 \times microscope objective lens was used to take a photomicrograph via ZEN 3.3 (blue edition) and IMAGE-PRO plus programme version 6.0 was used for measurement. Patterns of central myelin portion, central myelin length, and depth of TZ were determined. This study was approved by the Faculty of Medicine, Chulalongkorn University IRB committee (IRB no. 712/64).

Determination of the length of central myelin portion (F) and depth of central myelin-peripheral myelin TZ (f) (Fig. 1)

On each photomicrograph (Fig. 1), 1) line A was drawn between the junction where nerve met the brainstem, 2) line F was drawn from the tip of the arch-shaped transitional zone continuing at the middle of the nerve bundles to line A, 3) line B was drawn between the junction where the central myelin met the peripheral myelin, 4) line f was drawn from the middle of line B to the tip of the arch-shaped TZ. In addition, the longest central myelin portion of each nerve was depicted. All measurements were executed 3 times by a single investigator to minimize intra- and inter-observer error.

Statistical analysis

Collected data were analysed with IBM SPSS version 22.0 (IBM Corp., Armonk, NY, USA). All distances were presented in mean and standard deviation. Pearson correlation coefficient, Spearman's rank correlation coefficient and scatter plot were used to de-

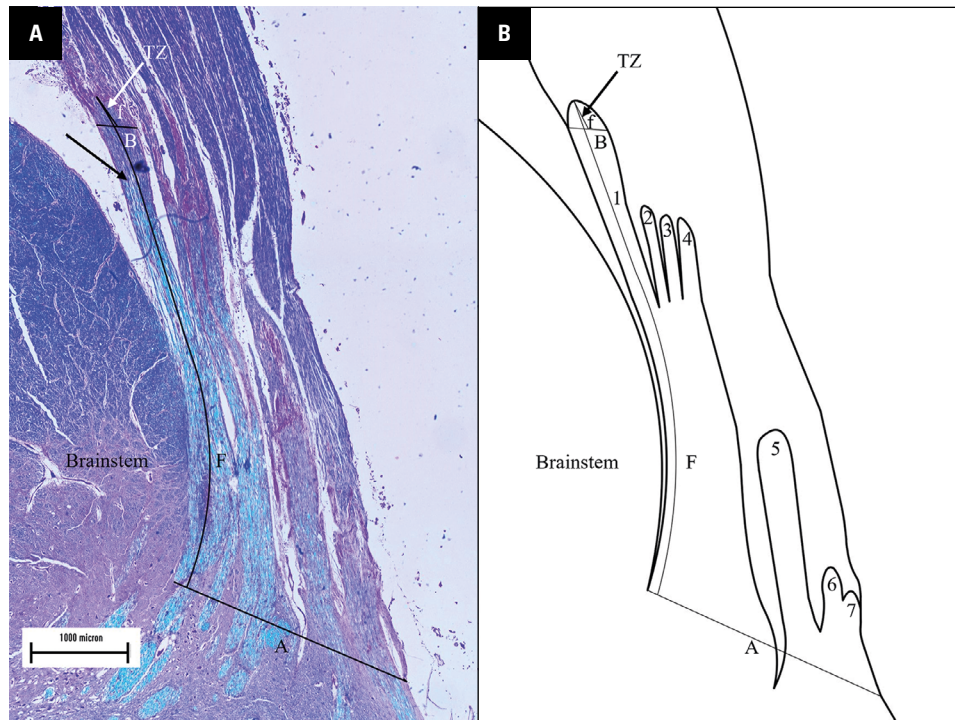


Figure 1. **A.** Photomicrograph of the oculomotor nerve stained with luxol fast blue demonstrates the longest central myelin seen at the first nerve bundle (black arrow) and then gradually decreased in length; **B.** Drawing demonstrating: **A** — a line drawn between junction where nerve met the brainstem; **B** — a line drawn between junction where central myelin met the peripheral myelin; **F** — length of central myelin of nerve bundle; **f** — depth of the transitional zone of the nerve bundle; **TZ** — transitional zone; 1, 2, 3, 4, 5, 6, 7 — order of the nerve bundle counted from the brainstem.

termine a correlation between depth of TZ and length of central myelin of each bundle. The significance level was set at a p-value of less than 0.05. Intra-observer reliability of each parameter was calculated.

RESULTS

Patterns of central myelin portion

Oculomotor nerve. The intramedullary rootlets of the oculomotor nerve united to form a single nerve trunk that emerged from the ventral surface of mid-brain. The extension of central myelin length differs between nerve bundles. We observed that the longest central myelin bundle was always seen on the first nerve bundle and that the length of central myelin decreased gradually (Fig. 1). Number of nerve bundles in each observed section was between 5 to 7 (Table 1).

Abducens nerve. The intramedullary rootlets of abducens nerve emerged from the ventral surface of the pontomedullary junction separately as one to three nerve rootlets. The one with two or three nerve rootlets united to form a single nerve trunk. The number of nerve bundles in each observed section was 1, 3, 4, and 5 (Table 2). The longest central myelin nerve bundle was found between the first to the third

nerve bundle with a prevalence of 30%, 30%, and 40%, respectively. Based on number of nerve rootlets emerging from the brainstem and number of nerve bundles in each rootlet, we classified morphologies of abducens nerve into four types (Fig. 2) — type A: single nerve rootlet with one nerve bundle, type B: single nerve rootlet with more than one nerve bundle, type C: more than one nerve rootlet with one nerve bundle in each nerve rootlet, and type D: more than one nerve rootlet with the most caudal nerve rootlet having more than one nerve bundle.

Lengths of central myelin portion (F) and the longest central myelin portion (F*)

Oculomotor nerve. The mean length of central myelin portion (F) measured from the nerve bundles in each nerve was 2.75 ± 0.83 mm (Table 1). When the whole nerve was considered, 80% of oculomotor nerves had a mean F of more than 2.00 mm for each nerve (Table 1, Fig. 3A). The mean longest central myelin portion (F*) of each nerve was 4.29 ± 1.26 mm (Table 1).

Abducens nerve. The mean F was 1.66 ± 1.39 mm (Table 2). When the whole nerve was considered, types A and B tended to have a longer segment of F

Table 1. All measurements of oculomotor nerves

Oculomotor nerve	No. of nerve bundles	F* [mm]	F [mm]	f [mm]
Nerve 1	5	3.01	2.23 ± 0.75 (1.28–3.01)	0.16 ± 0.03 (0.13–0.20)
Nerve 2	6	3.22	2.24 ± 1.06 (0.64–3.22)	0.14 ± 0.04 (0.11–0.21)
Nerve 3	7	2.76	1.57 ± 0.97 (0.51–2.76)	0.19 ± 0.04 (0.13–0.23)
Nerve 4	7	5.11	3.33 ± 1.05 (2.14–5.11)	0.18 ± 0.06 (0.09–0.26)
Nerve 5	5	3.37	1.95 ± 0.96 (1.18–3.37)	0.34 ± 0.17 (0.19–0.58)
Nerve 6	6	6.10	3.99 ± 1.59 (2.12–6.10)	0.33 ± 0.11 (0.24–0.53)
Nerve 7	7	3.76	2.67 ± 0.91 (1.54–3.76)	0.27 ± 0.05 (0.20–0.32)
Nerve 8	6	5.21	3.78 ± 1.07 (2.33–5.21)	0.24 ± 0.13 (0.11–0.43)
Nerve 9	7	4.28	2.34 ± 1.57 (0.36–4.28)	0.20 ± 0.07 (0.09–0.28)
Nerve 10	7	6.10	3.44 ± 1.60 (1.92–6.10)	0.25 ± 0.14 (0.07–0.50)
Mean ± SD (range)		4.29 ± 1.26 (2.76–6.10)	2.75 ± 0.83 (0.36–6.10)	0.23 ± 0.07 (0.07–0.58)
Shrinkage correction (range)		3.31–7.32		0.08–0.70

F — length of central myelin; F* — longest central myelin; f — depth of transitional zone; SD — standard deviation

Table 2. All measurements of abducens nerves

Abducens nerve	No. of nerve bundles	Morphological pattern	F* [mm]	F [mm]	f [mm]
Nerve 1	1	A	2.00	2.00	0.14
Nerve 2	3	B	2.29	2.26 ± 0.03 (2.23–2.29)	0.21 ± 0.02 (0.20–0.24)
Nerve 3	3	B	5.01	4.76 ± 0.28 (4.46–5.01)	0.23 ± 0.02 (0.22–0.24)
Nerve 4	3	C	0.53	0.36 ± 0.21 (0.13–0.53)	0.13 ± 0.13 (0.05–0.27)
Nerve 5	5	B	3.01	2.80 ± 0.28 (2.31–3.01)	0.10 ± 0.05 (0.06–0.17)
Nerve 6	3	C	1.00	0.63 ± 0.33 (0.37–1.00)	0.17 ± 0.03 (0.15–0.20)
Nerve 7	4	D	1.73	0.35 ± 0.32 (1.03–1.73)	0.15 ± 0.06 (0.08–0.22)
Nerve 8	4	D	0.86	0.62 ± 0.23 (0.37–0.86)	0.10 ± 0.02 (0.08–0.13)
Nerve 9	3	B	2.03	1.56 ± 0.68 (0.79–2.03)	0.30 ± 0.10 (0.23–0.41)
Nerve 10	3	C	0.28	0.21 ± 0.06 (0.16–0.28)	0.07 ± 0.01 (0.06–0.07)
Mean ± SD (range)			1.88 ± 1.40 (0.28–5.01)	1.66 ± 1.39 (0.13–5.01)	0.16 ± 0.07 (0.05–0.40)
Shrinkage correction (range)			0.34–6.01		0.06–0.48

F — length of central myelin; F* — longest central myelin; f — depth of transitional zone; SD — standard deviation

than type C and D (Table 2, Fig. 3B). The mean longest central myelin portion (F*) of each nerve was 1.88 ± 1.40 mm (Table 2).

Depths of central myelin-peripheral myelin TZ (f)

The mean depth of TZ (f) of oculomotor nerve was 0.23 ± 0.07 mm (Table 1). For abducens nerve, mean f was 0.16 ± 0.07 mm (Table 2).

Correlation between depth of TZ and length of central myelin

We found a positive weak correlation between f and F in oculomotor nerve by Pearson's correlation coefficient ($r +0.310$, $p < 0.05$). While using

Spearman's rank correlation coefficient, we found a positive weak correlation between f and F of each nerve bundle in abducens nerves ($r +0.413$, $p < 0.05$; Fig. 4).

Intra-observer intraclass correlation coefficient was 0.996 (0.992–1.000) for oculomotor nerve measurement and 0.998 (0.995–1.000) for abducens nerve measurement. The least intra-observer intraclass correlation coefficient among all parameters was 0.992.

DISCUSSION

The morphological pattern and number of nerve bundles of oculomotor and abducens nerves has never been described before. For oculomotor nerve,

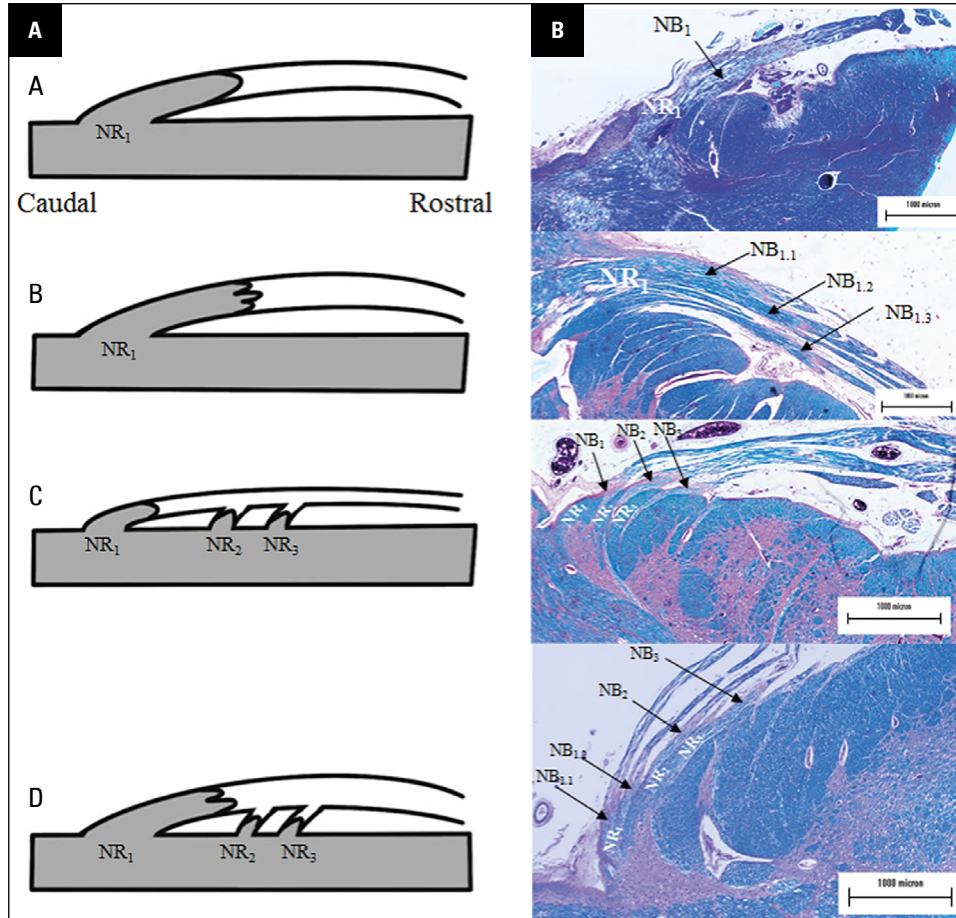


Figure 2. A. Schematic diagram demonstrates types of abducens nerve; B. Photomicrographs of abducens nerves stained with luxol fast blue demonstrate types of abducens nerve corresponding to the schematic diagram; A, B, C and D are types of abducens nerve; NR₁, NR₂, NR₃ — the first, second, and third nerve rootlet emerging from the ventral surface of brainstem; NB₁, NB₂, NB₃ — nerve bundle in the first, second and third nerve rootlets; NB_{1.1}, NB_{1.2}, NB_{1.3} — number of nerve bundle in the first nerve rootlet.

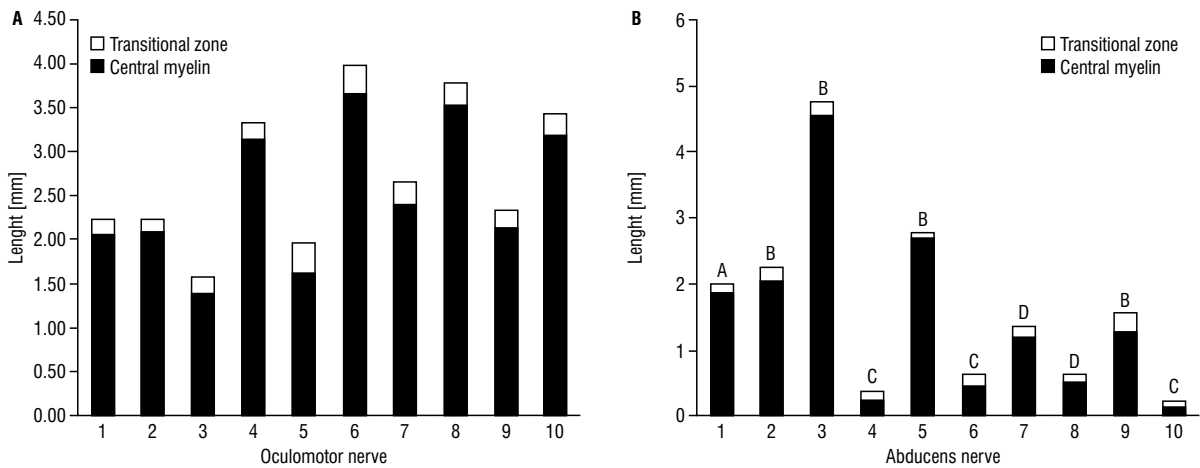


Figure 3. Bar graph showing mean value of central myelin portion (black) and depth of transitional zone (white) of 10 oculomotor (A) and 10 abducens nerves (B). Each bar represents each nerve. The letters A, B, C and D at the end of the graph of abducens nerves represent the morphology type of abducens nerves.

the longest central myelin was always seen on the first nerve bundle and the length of glial segment

decreased gradually. However, Fraher (1992) [5] who studied type of TZ in rats showed a similar central

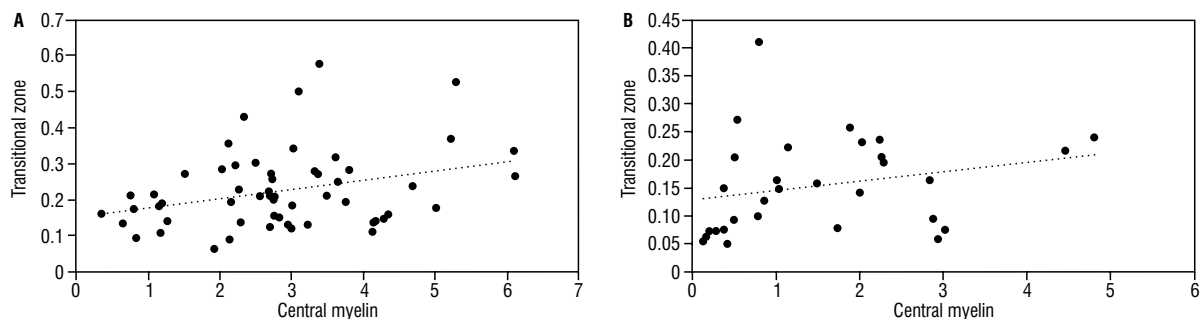


Figure 4. Scatter plot showing a correlation between central myelin portion and depth of transitional zone of each nerve bundle of oculomotor nerves (A) and abducens nerves (B).

myelin pattern and multiple nerve bundles in the schematic diagram of oculomotor nerves. For abducens nerve, the morphologies of the nerve bundle are classified into four types (A–D) based on the number of nerve rootlets and the number of nerve bundles. Fraher (1992) [5] also showed the same schematic diagram of abducens nerves having more nerve rootlets and one nerve bundle in each rootlet, similar to that found in the type C pattern in our study. Different positions of TZ could be explained by CNS and PNS tissue migration during development [5]. The morphological pattern of central myelin and appearance of TZ observed in this study were different from previous studies in other cranial nerves which always shows only one arch-shaped TZ [8, 9, 17, 20, 22, 25, 27]. Consequently, the measuring method in this study were designed to suit the pattern.

Skinner (1931) [22] is the first to demonstrate that length of glial part of oculomotor and abducens nerve from humans, dogs, cats, and rabbits were 1.2 and 0.5 mm, respectively. Tarlov (1937) [25] reported length of glial part of oculomotor and abducens nerve from humans were 0.6 and 0.5 mm, respectively. While our study found that lengths of central myelin are longer than previously reported for both cranial nerves. The oculomotor nerve had a greater length of central myelin when compared to abducens nerve in our study. This finding is consistent with Skinner [22] and Tarlov [25]. However, exact lengths cannot be compared because the definition of glial part was not mentioned and some nerve specimens were from animals. When the entire nerve was considered, most central myelin length of oculomotor nerves was between 2.00 and 4.00 mm (Fig. 3A). Furthermore, abducens nerve types A and B tend to have a longer segment of mean central myelin than types C and D (Fig. 3B). These findings could be

a benefit in neuroimaging interpretation. In cadaveric study, after specimens had been fixed, there were some shrinkages. Before applying in the clinical setting, this shrinkage must be taken into consideration. Estimated post fixation shrinkage has been reported up to 20% [29], therefore the corrected longest length of central myelin (F^*) would be 3.31–7.32 mm for oculomotor nerve and 0.34–6.02 mm for abducens nerve (Tables 1, 2).

The depth of TZ would be 0.08–0.70 mm for oculomotor nerve and 0.06–0.48 mm for abducens nerve (Tables 1, 2) if considering post fixation shrinkage [29]. TZ started from 3.03 (1.65–4.39) and 1.79 (0.17–5.44) mm distal to where the cranial nerve exits the brainstem for oculomotor and abducens nerves, respectively. Knowing the starting point of TZ could be useful in the localisation of compressed sites in neuroimaging. Moreover, we found a positive weak correlation between the depth of transitional zone and length of central myelin of each nerve bundle in the oculomotor and abducens nerves which could imply that the greater the central myelin, the greater the transitional zone depth.

Limitations of the study

Our study had a few limitations. First, cranial nerves in this study were harvested from brain collection, so age, sex, underlying disease, and cause of death of the cadavers are unknown. Second, we could not analyse the difference between sides due to the small number of specimens. Third, our results cannot be compared to other studies because of different measurement method.

CONCLUSIONS

In conclusion, this study provides details of micro-anatomical knowledge of oculomotor and abducens

nerves. Knowing the length of the central myelin and depth of TZ would be helpful in the localisation of compressed sites in neuroimaging. Moreover, this might help to understand the aetiology of ONM and CN VI palsy from neurovascular compression.

Acknowledgements

The authors would like to express our sincere appreciation to all those who have donated their bodies for medical study and research. Special thanks are extended to the technical staffs of the Department of Anatomy, Faculty of Medicine, Chulalongkorn University for their support in cadaveric care. This manuscript was edited by English editing service, Research Affairs, Faculty of Medicine, Chulalongkorn University.

Conflict of interest: None declared

REFERENCES

- Bojrab D, Zhang B, Jiang H, et al. Expression of oligodendrocyte marker during peripheral-central transitional zone formation of the postnatal mouse cochlear nerve. *Otolaryngol Head Neck Surg.* 2017; 157(3): 488–492, doi: [10.1177/0194599817718806](https://doi.org/10.1177/0194599817718806), indexed in Pubmed: [28695768](https://pubmed.ncbi.nlm.nih.gov/28695768/).
- De Ridder D, Menovsky T. Neurovascular compression of the abducent nerve causing abducent palsy treated by microvascular decompression. Case report. *J Neurosurg.* 2007; 107(6): 1231–1234, doi: [10.3171/JNS-07/12/1231](https://doi.org/10.3171/JNS-07/12/1231), indexed in Pubmed: [18077964](https://pubmed.ncbi.nlm.nih.gov/18077964/).
- De Ridder D, Møller A, Verlooy J, et al. Is the root entry/exit zone important in microvascular compression syndromes? *Neurosurgery.* 2002; 51(2): 427–433, doi: [10.1097/00006123-200208000-00023](https://doi.org/10.1097/00006123-200208000-00023), indexed in Pubmed: [12182781](https://pubmed.ncbi.nlm.nih.gov/12182781/).
- Elder C, Hainline C, Galetta SL, et al. Isolated abducens nerve palsy: update on evaluation and diagnosis. *Curr Neurol Neurosci Rep.* 2016; 16(8): 69, doi: [10.1007/s11910-016-0671-4](https://doi.org/10.1007/s11910-016-0671-4), indexed in Pubmed: [27306521](https://pubmed.ncbi.nlm.nih.gov/27306521/).
- Fraher JP. The CNS-PNS transitional zone of the rat. Morphometric studies at cranial and spinal levels. *Prog Neurobiol.* 1992; 38(3): 261–316, doi: [10.1016/0301-0082\(92\)90022-7](https://doi.org/10.1016/0301-0082(92)90022-7), indexed in Pubmed: [1546164](https://pubmed.ncbi.nlm.nih.gov/1546164/).
- Giray S, Pelit A, Kizilkilic O, et al. Isolated abducens nerve palsy caused by contralateral vertebral artery dolichoectasia. *Neurol India.* 2005; 53(2): 246–247, doi: [10.4103/0028-3886.16433](https://doi.org/10.4103/0028-3886.16433), indexed in Pubmed: [16010080](https://pubmed.ncbi.nlm.nih.gov/16010080/).
- Goldenberg-Cohen N, Miller NR. Noninvasive neuroimaging of basilar artery dolichoectasia in a patient with an isolated abducens nerve paresis. *Am J Ophthalmol.* 2004; 137(2): 365–367, doi: [10.1016/S0002-9394\(03\)00898-5](https://doi.org/10.1016/S0002-9394(03)00898-5), indexed in Pubmed: [14962438](https://pubmed.ncbi.nlm.nih.gov/14962438/).
- Guclu B, Sindou M, Meyronet D, et al. Anatomical study of the central myelin portion and transitional zone of the vestibulocochlear nerve. *Acta Neurochir (Wien).* 2012; 154(12): 2277–2283, doi: [10.1007/s00701-012-1479-x](https://doi.org/10.1007/s00701-012-1479-x), indexed in Pubmed: [22914910](https://pubmed.ncbi.nlm.nih.gov/22914910/).
- Guclu B, Sindou M, Meyronet D, et al. Cranial nerve vascular compression syndromes of the trigeminal, facial and vago-glossopharyngeal nerves: comparative anatomical study of the central myelin portion and transitional zone; correlations with incidences of corresponding hyperactive dysfunctional syndromes. *Acta Neurochir (Wien).* 2011; 153(12): 2365–2375, doi: [10.1007/s00701-011-1168-1](https://doi.org/10.1007/s00701-011-1168-1), indexed in Pubmed: [21947457](https://pubmed.ncbi.nlm.nih.gov/21947457/).
- Inoue T, Hirai H, Shimizu T, et al. Ocular neuromyotonia treated by microvascular decompression: usefulness of preoperative 3D imaging: case report. *J Neurosurg.* 2012; 117(6): 1166–1169, doi: [10.3171/2012.9.JNS112361](https://doi.org/10.3171/2012.9.JNS112361), indexed in Pubmed: [23020768](https://pubmed.ncbi.nlm.nih.gov/23020768/).
- Jannetta PJ. Neurovascular compression in cranial nerve and systemic disease. *Ann Surg.* 1980; 192(4): 518–525, doi: [10.1097/0000658-198010000-00010](https://doi.org/10.1097/0000658-198010000-00010), indexed in Pubmed: [6968543](https://pubmed.ncbi.nlm.nih.gov/6968543/).
- Jeeva-Patel T, Margolin EA, Mandell D. Sixth cranial nerve palsy secondary to compression by dolichoectatic verte-brobasilar artery. *BMJ Case Rep.* 2020; 13(7), doi: [10.1136/bcr-2020-234949](https://doi.org/10.1136/bcr-2020-234949), indexed in Pubmed: [32636226](https://pubmed.ncbi.nlm.nih.gov/32636226/).
- Kato H, Nakajima M, Ohnaka Y, et al. Recurrent abducens nerve palsy associated with neurovascular compression. *J Neurol Sci.* 2010; 295(1-2): 135–136, doi: [10.1016/j.jns.2010.05.001](https://doi.org/10.1016/j.jns.2010.05.001), indexed in Pubmed: [20621803](https://pubmed.ncbi.nlm.nih.gov/20621803/).
- Kiernan J. Histochemistry of staining methods for normal and degenerating myelin in the central and peripheral nervous systems. *J Histotechnol.* 2013; 30(2): 87–106, doi: [10.1179/his.2007.30.2.87](https://doi.org/10.1179/his.2007.30.2.87).
- Madhugiri VS, Roopesh Kumar VR, Gopalakrishnan MS, et al. Cranial polyneuropathy associated with verte-brobasilar dolichoectasia. *Clin Neurol Neurosurg.* 2012; 114(7): 1059–1061, doi: [10.1016/j.clineuro.2012.02.002](https://doi.org/10.1016/j.clineuro.2012.02.002), indexed in Pubmed: [22386900](https://pubmed.ncbi.nlm.nih.gov/22386900/).
- Narai H, Manabe Y, Deguchi K, et al. Isolated abducens nerve palsy caused by vascular compression. *Neurology.* 2000; 55(3): 453–454, doi: [10.1212/wnl.55.3.453](https://doi.org/10.1212/wnl.55.3.453), indexed in Pubmed: [10932293](https://pubmed.ncbi.nlm.nih.gov/10932293/).
- Nomura K, Ryu H, Ohno K, et al. Wide distribution of central myelin segment along the facial nerve might explain hemifacial spasm with distal nerve compression. *Clin Anat.* 2021; 34(3): 405–410, doi: [10.1002/ca.23664](https://doi.org/10.1002/ca.23664), indexed in Pubmed: [32713009](https://pubmed.ncbi.nlm.nih.gov/32713009/).
- Ohhashi G, Irie K, Tani S, et al. [Isolated abducens nerve palsy caused by the compression of the basilar artery: a case report]. *No To Shinkei.* 2001; 53(1): 69–72, indexed in Pubmed: [11211735](https://pubmed.ncbi.nlm.nih.gov/11211735/).
- Ohtsuka K, Sone A, Igarashi Y, et al. Vascular compressive abducens nerve palsy disclosed by magnetic resonance imaging. *Am J Ophthalmol.* 1996; 122(3): 416–419, doi: [10.1016/S0002-9394\(14\)72068-9](https://doi.org/10.1016/S0002-9394(14)72068-9), indexed in Pubmed: [8794714](https://pubmed.ncbi.nlm.nih.gov/8794714/).
- Peker S, Kurtkaya O, Uzün I, et al. Microanatomy of the central myelin-peripheral myelin transition zone of the trigeminal nerve. *Neurosurgery.* 2006; 59(2): 354–359, doi: [10.1227/01.NEU.0000223501.27220.69](https://doi.org/10.1227/01.NEU.0000223501.27220.69), indexed in Pubmed: [16883175](https://pubmed.ncbi.nlm.nih.gov/16883175/).
- Pham T, Wesolowski J, Trobe JD. Sixth cranial nerve palsy and ipsilateral trigeminal neuralgia caused by verte-brobasilar dolichoectasia. *Am J Ophthalmol Case Rep.* 2018; 10: 229–232, doi: [10.1016/j.ajoc.2018.02.029](https://doi.org/10.1016/j.ajoc.2018.02.029), indexed in Pubmed: [29780939](https://pubmed.ncbi.nlm.nih.gov/29780939/).

22. Skinner HA. Some histologic features of the cranial nerves. *Arch Neurol Psychiatry*. 1931; 25(2): 356, doi: [10.1001/archneurpsyc.1931.02230020144008](https://doi.org/10.1001/archneurpsyc.1931.02230020144008).
23. Stockman AC, Dieltiens M, Janssens H, et al. Ocular neuromyotonia: case reports and literature review. *Strabismus*. 2018; 26(3): 133–141, doi: [10.1080/09273972.2018.1467469](https://doi.org/10.1080/09273972.2018.1467469), indexed in Pubmed: [29693497](https://pubmed.ncbi.nlm.nih.gov/29693497/).
24. Tarlov IM. Structure of the nerve root. I. Nature of the junction between the central and the peripheral nervous system. *Arch Neurol Psychiatry*. 1937; 37(3): 555–583, doi: [10.1001/archneurpsyc.1937.02260150085005](https://doi.org/10.1001/archneurpsyc.1937.02260150085005).
25. Tarlov IM. Structure of the nerve root. II. Differentiation of sensory from motor roots; observations on identification of function in roots of mixed cranial nerves. *Arch Neurol Psychiatry*. 1937; 37(6): 1338–1355, doi: [10.1001/archneurpsyc.1937.02260180118008](https://doi.org/10.1001/archneurpsyc.1937.02260180118008).
26. Tilikete C, Vial C, Niederlaender M, et al. Idiopathic ocular neuromyotonia: a neurovascular compression syndrome? *J Neurol Neurosurg Psychiatry*. 2000; 69(5): 642–644, doi: [10.1136/jnnp.69.5.642](https://doi.org/10.1136/jnnp.69.5.642), indexed in Pubmed: [11032618](https://pubmed.ncbi.nlm.nih.gov/11032618/).
27. Tomii M, Onoue H, Yasue M, et al. Microscopic measurement of the facial nerve root exit zone from central glial myelin to peripheral Schwann cell myelin. *J Neurosurg*. 2003; 99(1): 121–124, doi: [10.3171/jns.2003.99.1.0121](https://doi.org/10.3171/jns.2003.99.1.0121), indexed in Pubmed: [12854753](https://pubmed.ncbi.nlm.nih.gov/12854753/).
28. Versino M, Colnaghi S, Todeschini A, et al. Ocular neuromyotonia with both tonic and paroxysmal components due to vascular compression. *J Neurol*. 2005; 252(2): 227–229, doi: [10.1007/s00415-005-0612-7](https://doi.org/10.1007/s00415-005-0612-7), indexed in Pubmed: [15729532](https://pubmed.ncbi.nlm.nih.gov/15729532/).
29. Yousry I, Moriggl B, Dieterich M, et al. MR anatomy of the proximal cisternal segment of the trochlear nerve: neurovascular relationships and landmarks. *Radiology*. 2002; 223(1): 31–38, doi: [10.1148/radiol.2231010612](https://doi.org/10.1148/radiol.2231010612), indexed in Pubmed: [11930045](https://pubmed.ncbi.nlm.nih.gov/11930045/).
30. Zhu Y, Thulborn K, Curnyn K, et al. Sixth cranial nerve palsy caused by compression from a dolichoectatic vertebral artery. *J Neuroophthalmol*. 2005; 25(2): 134–135, doi: [10.1097/01.wno.0000165319.75310.5a](https://doi.org/10.1097/01.wno.0000165319.75310.5a), indexed in Pubmed: [15937439](https://pubmed.ncbi.nlm.nih.gov/15937439/).